

Multipartite entanglement and one-way steering in magnon frequency comb

Qianjun Zheng(郑芊君), Yunshan Cao(曹云姗), and Peng Yan(严鹏)
Citation: Chin. Phys. B, 2025, 34 (**10**): 107514. DOI: 10.1088/1674-1056/adf9fe
http://cpb.iphy.ac.cn; http://iopscience.iop.org/cpb

What follows is a list of articles you may be interested in

Deformation of magnetic skyrmion due to skyrmion-skyrmion interaction

Zhen-Qian Cui(崔振茜), Wen-Li Yang(杨文力), and Jun-Hui Zheng(郑俊辉)
Chin. Phys. B, 2025, 34 (**7**): 077502. DOI: 10.1088/1674-1056/adca20

Strain-manipulated dispersion characteristics of magnonic crystals with Dzyaloshinskii-Moriya interaction and applications on spin-wave devices

Chuhan Zhou(周楚涵), Xiaotian Jiao(焦晓天), Jiaxi Xu(徐佳熙), Zhaonian Jin(金兆年), Lin Chen(陈琳), and Zhikuo Tao(陶志阔)
Chin. Phys. B, 2025, 34 (**2**): 027501. DOI: 10.1088/1674-1056/ad9892

Dzyaloshinskii-Moriya interaction and field-free sub-10 nm topological magnetism in Fe/bismuth oxychalcogenides heterostructures

Yaoyuan Wang(王垚元), Long You(游龙), Kai Chang(常凯), and Hongxin Yang(杨洪新)
Chin. Phys. B, 2024, 33 (**9**): 097508. DOI: 10.1088/1674-1056/ad6a0e

Frequency combs based on magnon-skyrmion interaction in magnetic nanotubes

Tijjani Abdulrazak, Xuejuan Liu(刘雪娟), Zhejunyu Jin(金哲珺雨), Yunshan Cao(曹云姗), and Peng Yan(严鹏)
Chin. Phys. B, 2024, 33 (**8**): 087503. DOI: 10.1088/1674-1056/ad4ff5

Shape-influenced non-reciprocal transport of magnetic skyrmions in nanoscale channel

Jie-Yao Chen(陈杰尧), Jia Luo(罗佳), Geng-Xin Hu(胡更新), Jun-Lin Wang(王君林), Guan-Qi Li(李冠祺), Zhen-Dong Chen(陈振东), Xian-Yang Lu(陆显扬), Guo-Ping Zhao(赵国平), Yuan Liu(刘远), Jing Wu(吴竞), and Yong-Bing Xu(徐永兵)
Chin. Phys. B, 2024, 33 (**7**): 077505. DOI: 10.1088/1674-1056/ad34c7

SPECIAL TOPIC — Advanced magnonics

Multipartite entanglement and one-way steering in magnon frequency comb

Qianjun Zheng(郑芊君), Yunshan Cao(曹云姗), and Peng Yan(严鹏)†

School of Physics and State Key Laboratory of Electronic Thin Films and Integrated Devices, University of Electronic Science and Technology of China, Chengdu 610054, *China*

(Received 12 June 2025; revised manuscript received 2 August 2025; accepted manuscript online 11 August 2025)

We theoretically demonstrate that multipartite entanglement and one-way Einstein–Podolsky–Rosen (EPR) steering in a magnon frequency comb (MFC) can be generated in a hybrid magnon–skyrmion system. When the system is driven by two microwave fields at the magnonic whispering gallery mode (mWGM) and the skyrmion, the skyrmion can be simultaneously entangled with three magnon modes of the MFC and the entanglement of the first-order magnon pair in the MFC also appears. The results show that the perfect one-way steering between the skyrmion and the three magnons can be obtained. Interestingly, the steering direction can be manipulated by controlling the amplitudes of two drive fields, which provides flexibility in controlling the asymmetry of the EPR steering and may well have practical applications. Moreover, the genuine tripartite entanglement among the skyrmion and the first-order magnon pair can be achieved with appropriate parameters in the steady state. Our work exhibits that the MFC has great potential in preparing multi-mode entanglement resources, with promising applications in quantum communication.

Keywords: multipartite entanglement, one-way steering, magnon frequency comb, skyrmion

PACS: 75.30.Ds, 03.67.Bg, 12.39.Dc

DOI: 10.1088/1674-1056/adf9fe **CSTR:** 32038.14.CPB.adf9fe

1. Introduction

Quantum entanglement is a key resource to operate quantum computers and ensure the security of quantum communication in quantum information science.[1–4] For two entangled particles, no matter how far apart they are, the state change of any particle will affect the state of the other particle by applying measurements, in which the status of both parties are equal. Different from that, Einstein–Podolsky–Rosen (EPR) steering,[5,6] as a strict subset of entanglement, exhibits an intrinsic property of the unequal status of two particles controlling the state of another particle, referred to as asymmetry. More attractive is one-way steering, where one party can steer the other by performing suitable measurements, but not vice versa. This property has been applied in one-sided device-independent quantum key distribution[7–9] and quantum networks.[10,11] Especially, multipartite entanglement and steering, with more complex characteristics than bipartite correlation, have significant potential for applications in constructing multi-node quantum communication networks and processing multi-party quantum information tasks.[12–16] In this context, the preparation and manipulation of multipartite entanglement is an important issue.

The optical frequency comb (OFC) consisting of a series of discrete and equally spaced frequency spectral lines has become an advantageous platform for studying multipartite quantum correlation, as a single fixed resource can produce multiple optical modes with different frequencies.[17] In 2011, Pysher *et al.*[18] simultaneously generated 15 quadripartite entangled cluster states in the OFC of a single optical parametric oscillator. In 2014, Chen *et al.*[19] experimentally realized the multipartite entanglement of 60 adjacent modes, which could be synchronously available and addressable in the OFC. In 2016, Reimer *et al.*[20] utilized an integrated Kerr OFC to achieve multiphoton entangled states, significantly advancing the practical application of OFC in quantum technology. Recently, the concept of the magnon frequency comb (MFC), analogous to the OFC, was proposed and has been observed in experiments.[21–25] Due to various nonlinear effects and the wide working frequency range of magnons, MFCs spanning from gigahertz (GHz) to terahertz (THz) and featuring hundreds of comb teeth have been theoretically suggested.[26–31] Wang *et al.*[21] were the first to theoretically predict the MFC through micromagnetic simulation based on the three-magnon scattering. As the primary nonlinear effect in magnetic systems, the three-magnon parametric interaction involves confluence and splitting processes,[31,32] essentially representing three-wave mixing. This physical mechanism for the generation of MFCs has been studied in various magnetic structures.[21,25–29] Hula *et al.*[22] experimentally observed the MFC generated by a

†Corresponding author. E-mail: yan@uestc.edu.cn

© 2025 Chinese Physical Society and IOP Publishing Ltd. All rights, including for text and data mining, AI training, and similar technologies, are reserved.

cascade four-magnon scattering process induced by two resonantly driven microwave fields. In this nonlinear parametric process, two excited magnons with different frequencies can simultaneously produce a high-frequency magnon and a low-frequency magnon,[33] which corresponds to four-wave mixing, with the comb spacing of the MFC determined by the frequency difference between the two driving fields. Moreover, the well-known nonlinear effect in cavity magnonic systems, the magnon Kerr effect, has been extensively studied in experiments.[34–37] This effect shares many similarities with the optical Kerr effect, as it is fundamentally four-wave mixing, one of which is that it can be used to generate MFCs. Wang *et al.*[38] demonstrated the controllable nonreciprocal MFC in a dual-cavity magnonic system, exploiting the asymmetric response of the magnon-Kerr nonlinearity to a microwave input from two different directions. Consequently, the MFC holds great promise as a candidate for preparing multipartite quantum entanglement resources in solid-state systems, offering strong potential for large-capacity and scalable quantum information storage and processing.

It is noteworthy that, very recently, multipartite entanglement involving up to 64 correlated modes in a microwave frequency comb has been generated through the three-wave mixing of a Josephson parametric amplifier.[39] Inspired by this, we have theoretically demonstrated that a topologically protected skyrmion with large dissipation can induce strong entanglement and asymmetric steering between the first-order magnon comb teeth in an MFC based on the nonlinear magnon–skyrmion interaction.[40] However, previous studies primarily focused on bipartite correlations between magnons with different frequencies, where the magnon driven by a microwave field was treated as a classical mode, and multimagnon entanglement was not taken into account. In this work, we try to reveal the multipartite correlation characteristics of an MFC by studying the quantum entanglement and steering among the skyrmion and the three magnon comb lines in the MFC, including the driven magnon and its nearest neighbor sum- and difference-frequency magnons. The theoretical model of our previous work[40] is still utilized, but the key difference is that the hybrid magnon–skyrmion system is driven by two microwave fields at the magnonic whispering gallery mode (mWGM) and the skyrmion. In this case, both the mWGM and the skyrmion will be excited and macroscopically occupied. The generation of the MFC does not require the driving field to exceed a threshold, and a similar mechanism has been investigated in antiferromagnets.[26]

When only the mWGM is resonantly driven by a microwave field, the difference-frequency magnon can be entangled with the skyrmion and the sum-frequency magnon, which is consistent with our previous work in the weak-coupling regime.[40] If the skyrmion is also driven and the quantum nature of the mWGM is considered, the entanglement between the skyrmion and the mWGM and the sum-frequency magnon arises. By controlling the amplitudes of the two driving fields, the skyrmion can be simultaneously entangled with the three magnons of the MFC and the entanglement between the first-order magnon comb teeth in the MFC can also exist. With the help of the effective Hamiltonian of the system, we analyze the underlying physical mechanism of multi-mode entanglement in detail from the perspective of entanglement transfer. The perfect one-way steering between the skyrmion and the three magnons is generated and the steering direction between the skyrmion and the sum- and difference-frequency magnons can be flexibly manipulated by changing the two driving amplitudes. Furthermore, a genuinely tripartite entangled state of the skyrmion, the sum-frequency magnon and the difference-frequency magnon can be prepared with appropriate driving amplitudes, which is robust against the environment thermal noises.

2. Theoretical model and system dynamics

We consider a hybrid magnon–skyrmion system consisting of a magnon waveguide and a skyrmion-microring resonator,[40] in which the incident mWGM $a_{\rm k}$ and the skyrmion breathing mode $a_{\rm r}$ are driven by two microwave fields with different frequencies ω_1, ω_2 and amplitude $\varepsilon_1, \varepsilon_2$, respectively. Without loss of generality, we investigate the multipartite quantum correlation among the skyrmion ($\omega_{\rm r}$) and represented by the three MFC teeth ($\omega_{\rm k}, \omega_{\rm p}, \omega_{\rm q}$), as shown in Fig. 1(a). The Hamiltonian describing the nonlinear magnon–skyrmion interaction in the system is written as ($\hbar = 1$)

$$
\begin{aligned}
&H = H_0 + H_{\rm int} + H_{\rm dr},\\
&H_0 = \omega_{\rm k} a_{\rm k}^{\dagger} a_{\rm k} + \omega_{\rm r} a_{\rm r}^{\dagger} a_{\rm r} + \omega_{\rm p} a_{\rm p}^{\dagger} a_{\rm p} + \omega_{\rm q} a_{\rm q}^{\dagger} a_{\rm q},\\
&H_{\rm int} = {\rm i} g_{\rm p} (a_{\rm k} a_{\rm r} a_{\rm p}^{\dagger} - a_{\rm k}^{\dagger} a_{\rm r}^{\dagger} a_{\rm p}) + {\rm i} g_{\rm q} (a_{\rm k} a_{\rm r}^{\dagger} a_{\rm q}^{\dagger} - a_{\rm k}^{\dagger} a_{\rm r} a_{\rm q}),\\
&H_{\rm dr} = {\rm i}\varepsilon_1 (a_{\rm k}^{\dagger} {\rm e}^{-{\rm i}\omega_1 t} - a_{\rm k} {\rm e}^{{\rm i}\omega_1 t}) + {\rm i}\varepsilon_2 (a_{\rm r}^{\dagger} {\rm e}^{-{\rm i}\omega_2 t} - a_{\rm r} {\rm e}^{{\rm i}\omega_2 t}),
\end{aligned} \tag{1}
$$

where $a_{\rm k,r,p,q}$ are the annihilation operators of the mWGM, the skyrmion, the sum-frequency and difference-frequency magnons. $\omega_{\rm k,r,p,q}$ are the resonant frequencies of the corresponding magnon modes, which satisfy $\omega_{\rm p} = \omega_{\rm k} + \omega_{\rm r}$ and $\omega_{\rm q} = \omega_{\rm k} - \omega_{\rm r}$. $g_{\rm p}$ and $g_{\rm q}$ are the magnon–skyrmion coupling strengths, respectively.

In the rotating frame at the frequency ω_1, the system Hamiltonian is simplified as

$$
\begin{aligned}
H \;=\; & \Delta_j a_j^{\dagger} a_j + \omega_{\rm r} a_{\rm r}^{\dagger} a_{\rm r} + {\rm i} g_{\rm p} (a_{\rm k} a_{\rm r} a_{\rm p}^{\dagger} - a_{\rm k}^{\dagger} a_{\rm r}^{\dagger} a_{\rm p})\\
& + {\rm i} g_{\rm q} (a_{\rm k} a_{\rm r}^{\dagger} a_{\rm q}^{\dagger} - a_{\rm k}^{\dagger} a_{\rm r} a_{\rm q})\\
& + {\rm i}\varepsilon_1 (a_{\rm k}^{\dagger} - a_{\rm k}) + {\rm i}\varepsilon_2 (a_{\rm r}^{\dagger} {\rm e}^{-{\rm i}\delta t} - a_{\rm r} {\rm e}^{{\rm i}\delta t}),
\end{aligned} \tag{2}
$$

where $\Delta_j = \omega_j - \omega_l$ $(j = \mathrm{k,p,q})$ and $\delta = \omega_2 - \omega_l$. In accordance with the magnon dissipation and environment noise, we can derive the quantum Langevin equations (QLEs) describing the system as follows:

$$\begin{aligned}
\dot{a}_\mathrm{k} &= -(\mathrm{i}\Delta_\mathrm{k} + \kappa_\mathrm{k})a_\mathrm{k} - g_\mathrm{p}a_\mathrm{r}^\dagger a_\mathrm{p} - g_\mathrm{q}a_\mathrm{r}a_\mathrm{q} + \varepsilon_l + \sqrt{2\kappa_\mathrm{k}}a_\mathrm{k}^\mathrm{in},\\
\dot{a}_\mathrm{r} &= -(\mathrm{i}\omega_\mathrm{r} + \kappa_\mathrm{r})a_\mathrm{r} - g_\mathrm{p}a_\mathrm{k}^\dagger a_\mathrm{p} + g_\mathrm{q}a_\mathrm{k}a_\mathrm{q}^\dagger + \varepsilon_2\mathrm{e}^{-\mathrm{i}\delta t} + \sqrt{2\kappa_\mathrm{r}}a_\mathrm{r}^\mathrm{in},\\
\dot{a}_\mathrm{p} &= -(\mathrm{i}\Delta_\mathrm{p} + \kappa_\mathrm{p})a_\mathrm{p} + g_\mathrm{p}a_\mathrm{k}a_\mathrm{r} + \sqrt{2\kappa_\mathrm{p}}a_\mathrm{p}^\mathrm{in},\\
\dot{a}_\mathrm{q} &= -(\mathrm{i}\Delta_\mathrm{q} + \kappa_\mathrm{q})a_\mathrm{q} + g_\mathrm{q}a_\mathrm{k}a_\mathrm{r}^\dagger + \sqrt{2\kappa_\mathrm{q}}a_\mathrm{q}^\mathrm{in},
\end{aligned} \tag{3}$$

where κ_j $(j = \mathrm{k,r,p,q})$ is the magnon dissipation coefficient, and a_j^in is the corresponding input noise operator, under the Markovian reservoir assumption, which are characterized by the zero-mean correlation functions: $\langle a_j^\mathrm{in}(t)a_j^{\mathrm{in}\dagger}(t')\rangle = [\bar{n}_j(\omega_j)+1]\delta(t-t')$, and $\langle a_j^{\mathrm{in}\dagger}(t)a_j^\mathrm{in}(t')\rangle = \bar{n}_j(\omega_j)\delta(t-t')$. The equilibrium mean thermal number of each mode $\bar{n}_j(\omega_j) = [\exp(\hbar\omega_j/\kappa_\mathrm{B}T)-1]^{-1}$, where T is the environment temperature and κ_B is the Boltzmann constant.

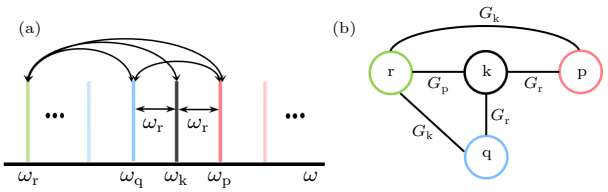


Fig. 1. (a) Schematic illustration of the multipartite entanglement among the skyrmion and different comb teeth in the MFC. (b) The effective interactions between different magnons.

When the system is in a steady state, the dynamics can be linearized around the steady-state values by writing the operators $a_j = \langle a_j\rangle + \delta a_j$ and neglecting the higher-order fluctuation terms. We can obtain the semi-classical equations for the magnon mean values

$$\begin{aligned}
\langle\dot{a}_\mathrm{k}\rangle &= -(\mathrm{i}\Delta_\mathrm{k} + \kappa_\mathrm{k})\langle a_\mathrm{k}\rangle - g_\mathrm{p}\langle a_\mathrm{r}^\dagger\rangle\langle a_\mathrm{p}\rangle - g_\mathrm{q}\langle a_\mathrm{r}\rangle\langle a_\mathrm{q}\rangle + \varepsilon_l,\\
\langle\dot{a}_\mathrm{r}\rangle &= -(\mathrm{i}\omega_\mathrm{r} + \kappa_\mathrm{r})\langle a_\mathrm{r}\rangle - g_\mathrm{p}\langle a_\mathrm{k}^\dagger\rangle\langle a_\mathrm{p}\rangle + g_\mathrm{q}\langle a_\mathrm{k}\rangle\langle a_\mathrm{q}^\dagger\rangle + \varepsilon_2\mathrm{e}^{-\mathrm{i}\delta t},\\
\langle\dot{a}_\mathrm{p}\rangle &= -(\mathrm{i}\Delta_\mathrm{p} + \kappa_\mathrm{p})\langle a_\mathrm{p}\rangle + g_\mathrm{p}\langle a_\mathrm{k}\rangle\langle a_\mathrm{r}\rangle,\\
\langle\dot{a}_\mathrm{q}\rangle &= -(\mathrm{i}\Delta_\mathrm{q} + \kappa_\mathrm{q})\langle a_\mathrm{q}\rangle + g_\mathrm{q}\langle a_\mathrm{k}\rangle\langle a_\mathrm{r}^\dagger\rangle.
\end{aligned} \tag{4}$$

For simplicity, we replace $\langle a_\mathrm{k}\rangle$, $\langle a_\mathrm{r}\rangle$, $\langle a_\mathrm{p}\rangle$, $\langle a_\mathrm{q}\rangle$ with A_k, $A_\mathrm{r}\mathrm{e}^{-\mathrm{i}\delta t}$, $A_\mathrm{p}\mathrm{e}^{-\mathrm{i}\delta t}$, $A_\mathrm{q}\mathrm{e}^{\mathrm{i}\delta t}$ so as to move into another interaction picture. The semi-class average equations are written by

$$\begin{aligned}
\dot{A}_\mathrm{k} &= -(\mathrm{i}\tilde{\omega}_\mathrm{k} + \kappa_\mathrm{k})A_\mathrm{k} - g_\mathrm{p}A_\mathrm{r}^*A_\mathrm{p} - g_\mathrm{q}A_\mathrm{r}A_\mathrm{q} + \varepsilon_l,\\
\dot{A}_\mathrm{r} &= -(\mathrm{i}\tilde{\omega}_\mathrm{r} + \kappa_\mathrm{r})A_\mathrm{r} - g_\mathrm{p}A_\mathrm{k}^*A_\mathrm{p} + g_\mathrm{q}A_\mathrm{k}A_\mathrm{q}^* + \varepsilon_2,\\
\dot{A}_\mathrm{p} &= -(\mathrm{i}\tilde{\omega}_\mathrm{p} + \kappa_\mathrm{p})A_\mathrm{p} + g_\mathrm{p}A_\mathrm{k}A_\mathrm{r},\\
\dot{A}_\mathrm{q} &= -(\mathrm{i}\tilde{\omega}_\mathrm{q} + \kappa_\mathrm{q})A_\mathrm{q} + g_\mathrm{q}A_\mathrm{k}A_\mathrm{r}^*,
\end{aligned} \tag{5}$$

where $\tilde{\omega}_\mathrm{k} = \Delta_\mathrm{k}, \tilde{\omega}_\mathrm{r} = \omega_\mathrm{r} - \delta, \tilde{\omega}_\mathrm{p} = \Delta_\mathrm{p} - \delta, \tilde{\omega}_\mathrm{q} = \Delta_\mathrm{q} + \delta$. Correspondingly, the linearized QLEs for quantum fluctuations are as follows:

$$\begin{aligned}
\dot{a}_\mathrm{k} &= -(\mathrm{i}\tilde{\omega}_\mathrm{k} + \kappa_\mathrm{k})a_\mathrm{k} - g_\mathrm{p}A_\mathrm{r}^*a_\mathrm{p} - g_\mathrm{p}A_\mathrm{p}a_\mathrm{r}^\dagger - g_\mathrm{q}A_\mathrm{r}a_\mathrm{q}\\
&\quad - g_\mathrm{q}A_\mathrm{q}a_\mathrm{r} + \sqrt{2\kappa_\mathrm{k}}a_\mathrm{k}^\mathrm{in},\\
\dot{a}_\mathrm{r} &= -(\mathrm{i}\tilde{\omega}_\mathrm{r} + \kappa_\mathrm{r})a_\mathrm{r} - g_\mathrm{p}A_\mathrm{k}^*a_\mathrm{p} - g_\mathrm{p}A_\mathrm{p}a_\mathrm{k}^\dagger\\
&\quad + g_\mathrm{q}A_\mathrm{k}a_\mathrm{q}^\dagger + g_\mathrm{q}A_\mathrm{q}^*a_\mathrm{k} + \sqrt{2\kappa_\mathrm{r}}a_\mathrm{r}^\mathrm{in},\\
\dot{a}_\mathrm{p} &= -(\mathrm{i}\tilde{\omega}_\mathrm{p} + \kappa_\mathrm{p})a_\mathrm{p} + g_\mathrm{p}A_\mathrm{k}a_\mathrm{r} + g_\mathrm{p}A_\mathrm{r}a_\mathrm{k} + \sqrt{2\kappa_\mathrm{p}}a_\mathrm{p}^\mathrm{in},\\
\dot{a}_\mathrm{q} &= -(\mathrm{i}\tilde{\omega}_\mathrm{q} + \kappa_\mathrm{q})a_\mathrm{q} - \mathrm{i}g_\mathrm{q}A_\mathrm{k}a_\mathrm{r}^\dagger - \mathrm{i}g_\mathrm{q}A_\mathrm{r}^*a_\mathrm{k} + \sqrt{2\kappa_\mathrm{q}}a_\mathrm{q}^\mathrm{in}.
\end{aligned} \tag{6}$$

If the driving frequencies satisfy $\omega_\mathrm{k} = \omega_l$ $(\tilde{\omega}_\mathrm{k} = \Delta_\mathrm{k} = 0)$ and $\delta = \omega_2 - \omega_l = \omega_\mathrm{r}$, then one can obtain $\tilde{\omega}_\mathrm{p} = \tilde{\omega}_\mathrm{r} = \tilde{\omega}_\mathrm{q} = 0$. The steady-state mean value solutions could be obtained from a set of semi-classical differential equations under the steady-state condition $\dot{A}_j = 0$. The equations are simplified as

$$\begin{aligned}
&\varepsilon_l - \kappa_\mathrm{k}A_\mathrm{k} - g_\mathrm{p}A_\mathrm{r}^*A_\mathrm{p} - g_\mathrm{q}A_\mathrm{r}A_\mathrm{q} = 0,\\
&\varepsilon_2 - \kappa_\mathrm{r}A_\mathrm{r} - g_\mathrm{p}A_\mathrm{k}^*A_\mathrm{p} + g_\mathrm{q}A_\mathrm{k}A_\mathrm{q}^* = 0,\\
&\kappa_\mathrm{p}A_\mathrm{p} - g_\mathrm{p}A_\mathrm{k}A_\mathrm{r} = 0,\\
&\kappa_\mathrm{q}A_\mathrm{q} - g_\mathrm{q}A_\mathrm{k}A_\mathrm{r}^* = 0.
\end{aligned} \tag{7}$$

The average values of magnons can all be real numbers by adjusting the two driving fields. By replacing $\delta a_\mathrm{k}, \delta a_\mathrm{r}, \delta a_\mathrm{p}, \delta a_\mathrm{q}$ with $a_\mathrm{k}, a_\mathrm{r}\mathrm{e}^{-\mathrm{i}\delta t}, a_\mathrm{p}\mathrm{e}^{-\mathrm{i}\delta t}, a_\mathrm{q}\mathrm{e}^{\mathrm{i}\delta t}$, the QLEs of the fluctuations are

$$\begin{aligned}
\dot{a}_\mathrm{k} &= -\kappa_\mathrm{k}a_\mathrm{k} - g_\mathrm{p}A_\mathrm{r}a_\mathrm{p} - g_\mathrm{p}A_\mathrm{p}a_\mathrm{r}^\dagger - g_\mathrm{q}A_\mathrm{r}a_\mathrm{q}\\
&\quad - g_\mathrm{q}A_\mathrm{q}a_\mathrm{r} + \sqrt{2\kappa_\mathrm{k}}a_\mathrm{k}^\mathrm{in},\\
\dot{a}_\mathrm{r} &= -\kappa_\mathrm{r}a_\mathrm{r} - g_\mathrm{p}A_\mathrm{k}a_\mathrm{p} - g_\mathrm{p}A_\mathrm{p}a_\mathrm{k}^\dagger + g_\mathrm{q}A_\mathrm{k}a_\mathrm{q}^\dagger\\
&\quad + g_\mathrm{q}A_\mathrm{q}a_\mathrm{k} + \sqrt{2\kappa_\mathrm{r}}a_\mathrm{r}^\mathrm{in},\\
\dot{a}_\mathrm{p} &= -\kappa_\mathrm{p}a_\mathrm{p} + g_\mathrm{p}A_\mathrm{k}a_\mathrm{r} + g_\mathrm{p}A_\mathrm{r}a_\mathrm{k} + \sqrt{2\kappa_\mathrm{p}}a_\mathrm{p}^\mathrm{in},\\
\dot{a}_\mathrm{q} &= -\kappa_\mathrm{q}a_\mathrm{q} - \mathrm{i}g_\mathrm{q}A_\mathrm{k}a_\mathrm{r}^\dagger - \mathrm{i}g_\mathrm{q}A_\mathrm{r}a_\mathrm{k} + \sqrt{2\kappa_\mathrm{q}}a_\mathrm{q}^\mathrm{in}.
\end{aligned} \tag{8}$$

By introducing the magnon position and momentum quadrature fluctuation operators $X_j = (\delta a_j + \delta a_j^\dagger)/\sqrt{2}$, $Y_j = \mathrm{i}(\delta a_j^\dagger - \delta a_j)/\sqrt{2}$, and the input noise quadrature operators $X_j^\mathrm{in} = (\delta a_j^\mathrm{in} + \delta a_j^{\mathrm{in}\dagger})/\sqrt{2}$, $Y_j^\mathrm{in} = \mathrm{i}(\delta a_j^{\mathrm{in}\dagger} - \delta a_j^\mathrm{in})/\sqrt{2}$, the linearized QLEs describing the quantum fluctuations can be rewritten as

$$\dot{\boldsymbol{u}}(t) = \boldsymbol{M}\boldsymbol{u}(t) + \boldsymbol{n}(t), \tag{9}$$

where the vector of the quadrature operators $\boldsymbol{u}(t) = [X_\mathrm{k}(t), Y_\mathrm{k}(t), X_\mathrm{r}(t), Y_\mathrm{r}(t), X_\mathrm{p}(t), Y_\mathrm{p}(t), X_\mathrm{q}(t), Y_\mathrm{q}(t)]^\mathrm{T}$, the noise vector $\boldsymbol{n}(t) = [\sqrt{2\kappa_\mathrm{k}}X_\mathrm{k}^\mathrm{in}, \sqrt{2\kappa_\mathrm{k}}Y_\mathrm{k}^\mathrm{in}, \sqrt{2\kappa_\mathrm{r}}X_\mathrm{r}^\mathrm{in}, \sqrt{2\kappa_\mathrm{r}}Y_\mathrm{r}^\mathrm{in}, \sqrt{2\kappa_\mathrm{p}}X_\mathrm{p}^\mathrm{in}, \sqrt{2\kappa_\mathrm{p}}Y_\mathrm{p}^\mathrm{in}, \sqrt{2\kappa_\mathrm{q}}X_\mathrm{q}^\mathrm{in}, \sqrt{2\kappa_\mathrm{q}}Y_\mathrm{q}^\mathrm{in}]^\mathrm{T}$, and $\boldsymbol{M}$ is the drift matrix

$$\boldsymbol{M}=\begin{pmatrix}
-\kappa_{\rm k} & 0 & -(g_{\rm p}A_{\rm p}+g_{\rm q}A_{\rm q}) & 0 & -g_{\rm p}A_{\rm r} & 0 & -g_{\rm q}A_{\rm r} & 0\\
0 & -\kappa_{\rm k} & 0 & g_{\rm p}A_{\rm p}-g_{\rm q}A_{\rm q} & 0 & -g_{\rm p}A_{\rm r} & 0 & -g_{\rm q}A_{\rm r}\\
g_{\rm q}A_{\rm q}-g_{\rm p}A_{\rm p} & 0 & -\kappa_{\rm r} & 0 & -g_{\rm p}A_{\rm k} & 0 & g_{\rm q}A_{\rm k} & 0\\
0 & g_{\rm p}A_{\rm p}+g_{\rm q}A_{\rm q} & 0 & -\kappa_{\rm r} & 0 & -g_{\rm p}A_{\rm k} & 0 & -g_{\rm q}A_{\rm k}\\
g_{\rm p}A_{\rm r} & 0 & g_{\rm p}A_{\rm k} & 0 & -\kappa_{\rm p} & 0 & 0 & 0\\
0 & g_{\rm p}A_{\rm r} & 0 & g_{\rm p}A_{\rm k} & 0 & -\kappa_{\rm p} & 0 & 0\\
g_{\rm q}A_{\rm r} & 0 & g_{\rm q}A_{\rm k} & 0 & 0 & 0 & -\kappa_{\rm q} & 0\\
0 & g_{\rm q}A_{\rm r} & 0 & -g_{\rm q}A_{\rm k} & 0 & 0 & 0 & -\kappa_{\rm q}
\end{pmatrix}. \tag{10}$$

If the real parts of all eigenvalues of $\boldsymbol{M}$ are negative, the system is stable and reaches a steady state, which can be derived by applying the Routh–Hurwitz criterion.[41] Because the dynamics of quadrature components fluctuations are linearized and the input noises are Gaussian, the system finally evolves into a zero-mean continuous variable (CV) Gaussian state that can be characterized by a 8×8 covariance matrix (CM) $\boldsymbol{V}$, where the matrix elements are defined as $\boldsymbol{V}_{kl}=\langle \boldsymbol{u}_k(\infty)\boldsymbol{u}_l(\infty)+\boldsymbol{u}_l(\infty)\boldsymbol{u}_{\rm k}(\infty)\rangle/2$ $(k,l=1,2,\ldots,8)$. When the system stability conditions are fulfilled, the steady-state CM $\boldsymbol{V}$ can be obtained by solving the Lyapunov equation[42]

$$\boldsymbol{M}\boldsymbol{V}+\boldsymbol{V}\boldsymbol{M}^{\rm T}=-D. \tag{11}$$

$\boldsymbol{D}=\mathrm{diag}[\kappa_{\rm k}(2\bar{n}_{\rm k}+1),\kappa_{\rm k}(2\bar{n}_{\rm k}+1),\kappa_{\rm r}(2\bar{n}_a+1),\kappa_{\rm r}(2\bar{n}_a+1),\kappa_{\rm p}(2\bar{n}_{\rm p}+1),\kappa_{\rm p}(2\bar{n}_{\rm p}+1),\kappa_{\rm q}(2\bar{n}_{\rm q}+1),\kappa_{\rm q}(2\bar{n}_{\rm q}+1)]$ is the diffusion matrix.

To quantitatively study the quantum correlation of the MFC in the multipartite CV system, we adopt the logarithmic negativity $E_{\rm N}$[43] and the Gaussian quantum steering[44] $S_{12}>0$ $(S_{12}>0)$ denotes that the bipartite Gaussian state is steerable from mode 1 (2) to mode 2 (1) by applying Gaussian measurements on mode 1 (2), and the larger of its value denotes the stronger Gaussian steerability. The minimal residual contangle $R_\tau^{\rm min}$[45] is used to quantify the genuine tripartite entanglement among any three modes, which is given by

$$R_\tau^{\rm min}\equiv \min[R_\tau^{i|jl},R_\tau^{j|il},R_\tau^{k|il}], \tag{12}$$

where the residual contangle $R_\tau^{i|jl}\equiv C_{i|jl}-C_{i|j}-C_{i|l}\geq 0$ $(i,j,l\in {\rm k,r,p,q})$ is a CV analogue of tangle for discrete-variable tripartite entanglement with $C_{u|v}=E_{u|v}^2$. When v contains two modes, $C_{i|jl}$ is calculated by extending the logarithmic negativity to three modes $E_{i|jl}$. The residual contangle satisfies the monogamy of quantum entanglement and $R_\tau^{i|jl}$ is a proper entanglement monotone; therefore, in terms of the case with $R_\tau^{\rm min}>0$, genuine tripartite entanglement is generated.

3. Results and discussion

In this section, we shall analyze the quantum correlation characteristics among the skyrmion, the mWGM, and the sum- and difference-frequency magnons through numerical simulation results. Firstly, we analyze the generation of bipartite entanglement of four magnon modes, then discuss the controlled EPR steering between the skyrmion and three magnon teeth in the MFC, and finally show the genuine tripartite entanglement among the skyrmion and the sum- and difference-frequency magnons. Here we assume $g_{\rm p}=g_{\rm q}=g$, $\kappa_{\rm p}=\kappa_{\rm q}=\kappa_{\rm pq}$ for simplicity, and the averages are

$$A_{\rm k}=\frac{\varepsilon_1}{\kappa_{\rm k}+2g^2/\kappa_{\rm pq}},\quad A_{\rm r}=\frac{\varepsilon_2}{\kappa_{\rm r}},\quad A_{\rm p}=A_{\rm q}=\frac{gA_{\rm k}A_{\rm r}}{\kappa_{\rm pq}}. \tag{13}$$

Then the effective Hamiltonian for the quantum fluctuations can be obtained as

$$\begin{aligned}H_{\rm eff}=\;&G_{\rm k}(a_{\rm r}^\dagger a_{\rm q}^\dagger+a_{\rm r}^\dagger a_{\rm p}+{\rm H.c.})+G_{\rm r}(a_{\rm k}^\dagger a_{\rm p}+a_{\rm k}a_{\rm q}^\dagger+{\rm H.c.})\\&+G_{\rm p}(a_{\rm k}^\dagger a_{\rm r}^\dagger+a_{\rm k}^\dagger a_{\rm r}+{\rm H.c.}),\end{aligned} \tag{14}$$

where $G_{\rm k}=gA_{\rm k}$, $G_{\rm r}=gA_{\rm r}$, $G_{\rm p}=gA_{\rm p}$ are effective coupling strengths, which can be significantly enhanced by the two driving fields. The effective interactions between different magnon modes in the system are shown in Fig. 1(b).

In Fig. 2, we plot the logarithmic negativity related to bipartite entanglements of four magnons $E_{\rm kr}$, $E_{\rm rp}$, $E_{\rm rq}$, $E_{\rm pq}$ as functions of two driving amplitudes ε_1 and ε_2. We take the parameters $\omega_{\rm k}/2\pi=80$ GHz, $\omega_{\rm p}/2\pi=88$ GHz, $\omega_{\rm q}/2\pi=72$ GHz, $\omega_{\rm r}/2\pi=8$ GHz, $g/2\pi=2$ MHz, $\kappa_{\rm k}/2\pi=4$ MHz, $\kappa_{\rm pq}/2\pi=1$ MHz, $\kappa_{\rm r}/2\pi=2$ MHz, $T=20$ mK.[21,40] It can be found that the skyrmion can be entangled with three magnon teeth of the MFC and the entanglement between the sum- and difference-frequency magnons can also be generated. From Fig. 2(a), we can see that the amplitude of two driving fields $\varepsilon_1\approx 0.4\times 10^8$ Hz and $\varepsilon_2\approx 0.12\times 10^8$ Hz are optimal for the mWGM-skyrmion entanglement $E_{\rm kr}$ where the maximum value of the entanglement is about 0.31. The entanglement between the skyrmion and the sum-frequency magnon $E_{\rm rp}$ is generated with the parameter interval of the driving $\varepsilon_1<0.5\times 10^8$ Hz, and it gradually increases with the enhancement of the driving ε_2, as shown in Fig. 2(b). From Figs. 2(c) and 2(d), it is found that the entanglement $E_{\rm rq}$ and $E_{\rm pq}$ exists when there is no driving ε_2 but only ε_1 $(\varepsilon_1\neq 0$, $\varepsilon_2=0)$. In this case, the corresponding effective Hamiltonian of the system is $H'_{\rm eff}=G_{\rm k}(a_{\rm r}^\dagger a_{\rm q}^\dagger+a_{\rm r}^\dagger a_{\rm p}+{\rm H.c.})$. The first parametric down-conversion interaction induces the entanglement

between the skyrmion and the difference-frequency magnon and it partially transfers to the other subsystem via the second beam–splitter interaction, resulting in the entanglement of the sum- and difference-frequency magnons. The entanglement mechanism is consistent with our previous work in the weak-coupling regime.[40] When the driving ε_2 is added in the system, these entanglements are evidently affected. In Fig. 2(c), the skyrmion and the difference-frequency magnon are hardly entangled with the parameters $\varepsilon_1 > 0.2\times10^8$ Hz, $\varepsilon_2 > 0.1\times10^8$ Hz. No matter how strong the driving ε_1 is, the entanglement $E_{\rm pq}$ almost disappears for $\varepsilon_2 = 0.1\times10^8$ Hz, as shown in Fig. 2(d). However, when the system has no driving ε_1, although the driving ε_2 exists, there is no entanglement at the stable state. From the corresponding effective Hamiltonian $H''_{\rm eff} = G_{\rm r}(a^\dagger_{\rm k}a_{\rm p} + a_{\rm k}a^\dagger_{\rm q} + {\rm H.c.})$, we can find that the linear interactions between the skyrmion and the sum (difference)-frequency magnon cannot generate any entanglement. It can be observed from Fig. 2 that entanglement transfer occurs in this system, in which the entanglement is distributed in different subsystems with the change of two driving amplitudes. That is to say, the driving ε_2 on the skyrmion not only reduces the experimental difficulty of generating an MFC,[26] but also becomes a method to manipulate the entanglement of different comb teeth in an MFC.

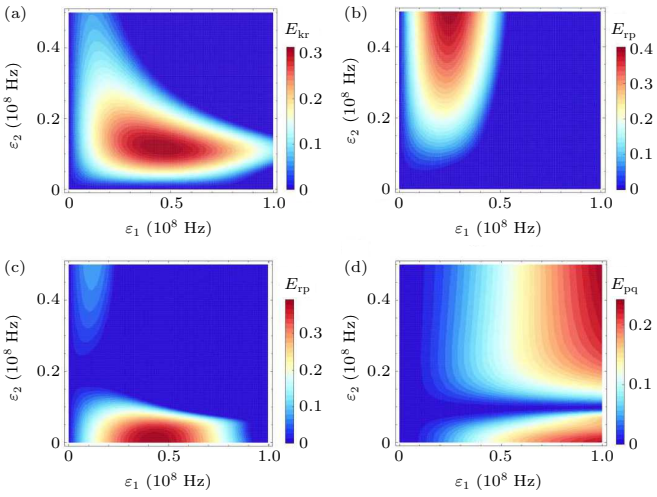


Fig. 2. Density plot of bipartite entanglements (a) $E_{\rm kr}$, (b) $E_{\rm rp}$, (c) $E_{\rm rq}$, and (d) $E_{\rm pq}$ versus the amplitudes of two driving fields ε_1 and ε_2.

In order to further analyze how the entanglement is transferred among different subsystems, we investigate the stationary four entanglements versus ε_1 with a fixed $\varepsilon_2 = 0.14\times10^8$ Hz and ε_2 with a fixed $\varepsilon_1 = 0.15\times10^8$ Hz, which are shown in Figs. 3(a) and 3(c), respectively. In Fig. 3(a), it is evident that all entanglements appear when $\varepsilon_1 > 0$. As the driving ε_1 increases, the entanglements $E_{\rm kr}$, $E_{\rm rp}$, $E_{\rm rq}$ begin to increase and then decrease in different degrees, yet the entanglement between the sum- and difference-magnons $E_{\rm pq}$ always maintains a rising trend. In Fig. 3(b), we show the effective coupling strengths $G_{\rm k}, G_{\rm r}, G_{\rm p}$ as the function of ε_1 to analyze the entanglement distribution in Fig. 3(a). It can be seen that $G_{\rm k}$ and $G_{\rm p}$ increase with the enhancement of ε_1, so the skyrmion is entangled with the mWGM and the difference-frequency magnon due to their parametric down-conversion couplings ($E_{\rm kr}, E_{\rm rq} > 0$). In the initial stage of ε_1 increasing, $G_{\rm r} > G_{\rm p} > G_{\rm k}$, thus the entanglement $E_{\rm kr}$ can be partially transferred to the subsystem of the skyrmion and the p-mode magnon via the state-swap interaction between the k-mode and p-mode magnons [the coupling channel $G_{\rm r}$ in Fig. 1(b)], leading to the entanglement $E_{\rm rp}$. Similarly, $E_{\rm rq}$ can be distributed to the p- and q-mode (r- and p-mode) magnon subsystem through the state-exchange coupling channel $G_{\rm k}$ of the r- and p-mode magnons ($G_{\rm r}$ of the p- and q-mode magnons mediated by the k-mode magnon). So we can see that the four entanglements gradually increase. As ε_1 continues to strengthen, the entanglement $E_{\rm rp(q)}$ will be transferred to $E_{\rm pq}$ via the coupling channel of the r- and q(p)-mode magnons mediated by the k-mode magnon, which corresponds to the decrease of $E_{\rm rp}$, $E_{\rm rq}$ and the increase of $E_{\rm pq}$. When the driving ε_1 is stronger, $G_{\rm p} > G_{\rm r} > G_{\rm k}$, the state-exchange interactions between the r-mode and the p-modes and q-mode magnons mediated by the k-mode magnon are enhanced and the entanglement $E_{\rm kr}$ as an entanglement source is transferred to the sum- and difference-frequency magnon subsystem, which corresponds to the decrease of $E_{\rm rp}$ and the increase of $E_{\rm pq}$. We then analyze the change of the four entanglements versus ε_2 in the same way. From Fig. 3(c), it can be found that $E_{\rm rq}, E_{\rm pq} > 0$ for the driving $\varepsilon_2 = 0$, which is consistent with Figs. 2(c) and 2(d). When ε_2 starts to increase, $G_{\rm r}, G_{\rm p}$ are enhanced, thus entanglement between the mWGM and the skyrmion $E_{\rm kr}$ is generated due to their parametric down-conversion coupling, and meanwhile $E_{\rm rq}$ is distributed to $E_{\rm kr}$ through the state-swap interaction between the k- and q-modes. In addition, $E_{\rm rq}$ is also transferred to $E_{\rm rp}$ via the coupling channel of the p-mode and q-mode magnons connected by the k-mode magnon. As shown in Fig. 3(c), with the enhancement of ε_2, the entanglement $E_{\rm rq}$ decreases and $E_{\rm kr}, E_{\rm rp}$ increase. As ε_2 continues to increase, $G_{\rm r} > G_{\rm p} > G_{\rm k}$ and the interactions between the k-mode and p(q)-mode magnons are strengthened. Consequently, $E_{\rm kr}$ can be partially transferred to the subsystem of the skyrmion and the sum- or difference-frequency magnons, which is characterized by the decrease of $E_{\rm kr}$ and the increase of $E_{\rm rp}, E_{\rm rq}$, and the four magnon modes are simultaneously entangled with each other. From the above qualitative analysis, it can be seen that, in such a complex multipartite system, the entanglement of magnons with different frequencies depends on the different effective interaction strengths among four modes, which can be directly controlled by changing the amplitudes of two driving field.

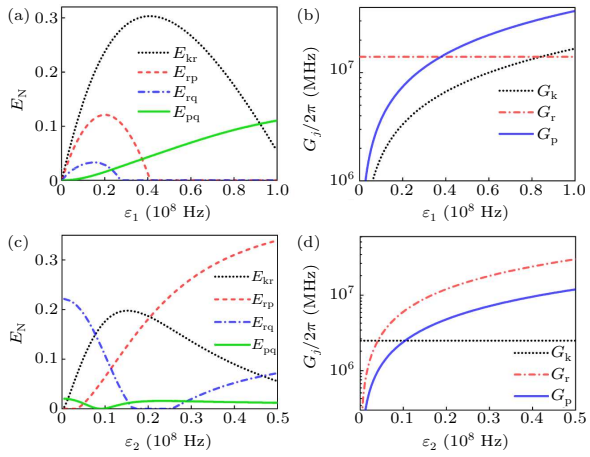


Fig. 3. Bipartite entanglement between four magnons versus (a) ε_1 and (c) ε_2. The effective coupling strengths G_k, G_r and G_p versus (b) ε_1 and (d) ε_2. $\varepsilon_2 = 0.14 \times 10^8$ Hz in panels (a)–(b) and $\varepsilon_1 = 0.15 \times 10^8$ Hz in panels (c)–(d).

Then we discuss the influence of some system parameters on the stationary bipartite entanglement and steering between the skyrmion and three magnon comb teeth. The quantum correlation E_{kr}, S_{kr}, S_{rk} between the skyrmion and the mWGM as functions of the ratio of two driving amplitudes $\varepsilon_1/\varepsilon_2$ with the fixed $\varepsilon_2 = 0.15 \times 10^8$ Hz are illustrated in Fig. 4(a). From Fig. 4(a), it can be found that the mWGM-skyrmion entanglement first increases and then decreases with the increase of ε_1, and disappears when $\varepsilon_1 > 6.85\varepsilon_2$. Interestingly, the one-way steering from the skyrmion to the mWGM can be generated with the parameter regime $0 < \varepsilon_1/\varepsilon_2 < 3$, which is numerically proved as $S_{rk} > 0, S_{kr} = 0$ (blue region). It indicates that the skyrmion can unidirectionally control the state of the mWGM by applying suitable measurement but not vice versa. The entanglement E_{kr} and steering S_{kr}, S_{rk} versus dissipation of the skyrmion γ_r and the mWGM γ_k with $\varepsilon_1 = 2\varepsilon_2$ are displayed in Figs. 4(b)–4(d), respectively. We can see that the one-way steering from the mWGM to the skyrmion S_{kr} can be prepared under the condition of small γ_k ($\gamma_k < 0.28\kappa_k$), as shown in Fig. 4(c). In contrast, one-way steering S_{rk} appears with large mWGM dissipation $\gamma_k > 0.7\kappa_k$ in Fig. 4(d). It is obvious that E_{kr}, S_{kr}, S_{rk} decrease with the addition of dissipation, which implies that magnon damping is harmful to entanglement and steering. However, the steering direction can be controlled by changing the magnon dissipation, as illustrated in Fig. 4(e). We can see that as the mWGM dissipation γ_k increases gradually, the one-way steering from k-mode to r-mode (red region), two-way unsteerable, and the one-way steering from r-mode to k-mode (blue region) correlations can be achieved in the system. In order to analyze how the directionality of quantum steering is affected by the asymmetric dissipation of two magnon modes, the effective magnon number can be introduced, which has been addressed in our previous work.[40] The smaller the dissipation of the magnon means the less it leaks from the system to the environment, so one mode with a larger number of magnons has more advantages in steering the other magnon mode. Therefore, when the dissipation of the mWGM is small, the steering is from the mWGM to the skyrmion [see Fig. 4(c)]; yet with the increase of the dissipation, the steering directionality is reversed from the skyrmion to the mWGM [see Figs. 4(d)]. Figure 4(f) shows the that mWGM-skyrmion entanglement is robust against the thermal fluctuation, surviving up to 0.64 K. The steerability is more sensitive to environmental temperature than to the entanglement, where one-way steering S_{rk} can exist when $T < 0.26$ K (blue region).

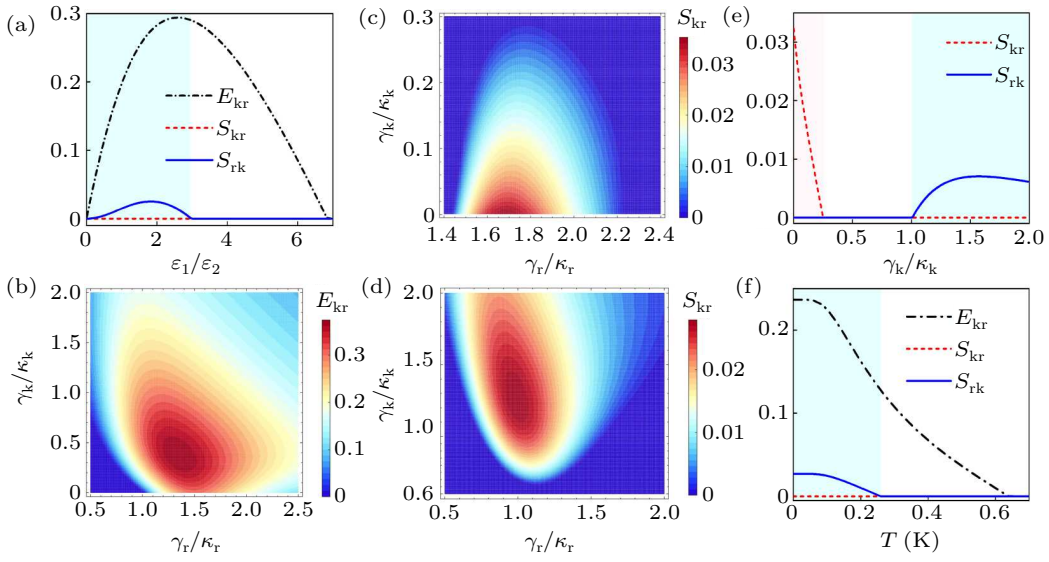


Fig. 4. (a) Bipartite entanglement E_{kr} and steering S_{kr} and S_{rk} between the mWGM and the skyrmion versus $\varepsilon_1/\varepsilon_2$. Density plot of (b) E_{kr}, (c) S_{kr} and (d) S_{rk} versus the dissipations of the skyrmion γ_r and the mWGM γ_k with $\varepsilon_1/\varepsilon_2 = 2$. (e) S_{kr} and S_{rk} versus γ_k with $\gamma_r = 1.6\kappa_r$. (f) Bipartite entanglement and steering versus temperature T with $\gamma_k = 1.4\kappa_k$ and $\gamma_r = \kappa_r$. The fixed driving amplitude $\varepsilon_2 = 0.15 \times 10^8$ Hz, $\kappa_r/2\pi = 2$ MHz and $\kappa_k/2\pi = 4$ MHz.

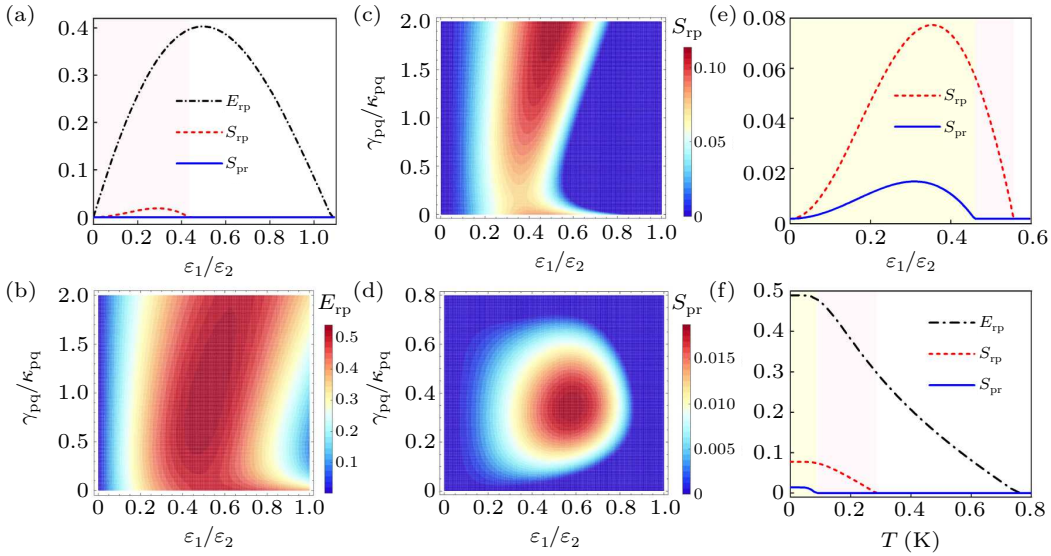


Fig. 5. (a) Bipartite entanglement E_{rp} and steering S_{rp} and S_{pr} between the skyrmion and the sum-frequency magnon modes versus the ratio of two driving amplitudes $\varepsilon_1/\varepsilon_2$. Density plot of (b) E_{rp}, (c) S_{rp} and (d) S_{pr} versus $\varepsilon_1/\varepsilon_2$ and the sum (difference)-frequency magnon dissipation γ_{pq} with $\kappa_r/2\pi = 1$ MHz and $\kappa_{pq}/2\pi = 1$ MHz. (e) S_{rp} and S_{pr} versus $\varepsilon_1/\varepsilon_2$ with $\gamma_{pq}/2\pi = 0.35\kappa_{pq}$. (f) Bipartite entanglement and steering versus temperature T with $\varepsilon_1 = 0.35\varepsilon_2$. The fixed driving amplitude $\varepsilon_2 = 0.5 \times 10^8$ Hz.

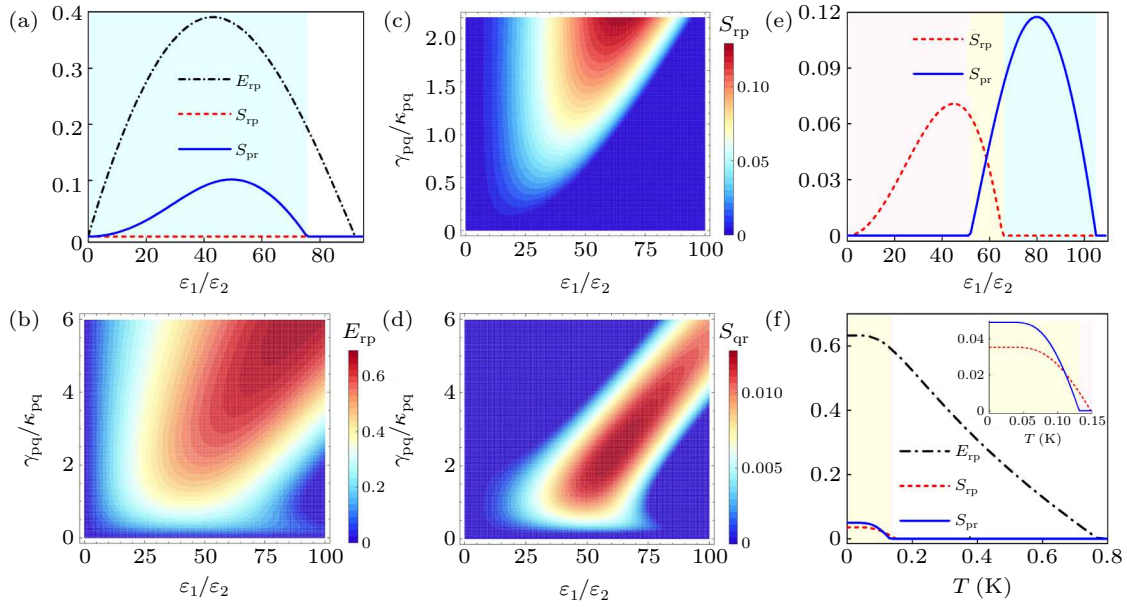


Fig. 6. (a) Bipartite entanglement E_{rq} and bipartite steering S_{rq} and S_{qr} between the skyrmion and the difference-frequency magnon modes versus $\varepsilon_1/\varepsilon_2$. Density plot of (b) bipartite entanglement E_{rq}, bipartite steering (c) S_{rq} and (d) S_{qr} versus $\varepsilon_1/\varepsilon_2$ and γ_{pq} with $\kappa_r/2\pi = 1$ MHz and $\kappa_{pq}/2\pi = 1$ MHz. (e) Bipartite asymmetric steering S_{rq} and S_{qr} versus $\varepsilon_1/\varepsilon_2$ with $\gamma_{pq}/2\pi = 4\kappa_{pq}$. (f) Bipartite entanglement and steering versus temperature T with $\varepsilon_1 = 60\varepsilon_2$. The fixed driving amplitude $\varepsilon_2 = 0.01 \times 10^8$ Hz.

Figure 5(a) exhibits the entanglement E_{rp} and steering S_{rp}, S_{pr} versus $\varepsilon_1/\varepsilon_2$ with $\varepsilon_2 = 0.5 \times 10^8$ Hz. When the driving $\varepsilon_1 < 1.08\varepsilon_2$, the stationary entanglement between the skyrmion and the sum-frequency magnon can be obtained and the one-way steering from the skyrmion to the sum-frequency magnon appears with the parameter regime $\varepsilon_1/\varepsilon_2 < 0.43$ ($S_{rp} > 0, S_{pr} = 0$, red region). Figures 5(b)–5(d) show the influence of the skyrmion dissipation on the entanglement and steering. It can be seen that the ability of the skyrmion to steer the p-mode magnon can be enhanced by increasing the sum(difference)-frequency magnon dissipation γ_{pq}. The p-mode magnon can steer the skyrmion with its smaller dissipation, specifically, $\gamma_{pq} < 0.7\kappa_{pq}$, which is demonstrated in Fig. 5(d). In other words, the magnon mode with larger damping is more difficult to steer the other one. It can be observed that the correlation degree of the entanglement is greater than the quantum steering for the same parameters regime ($E_{rp} > S_{rp}, S_{pr}$) and both S_{rp}, S_{pr} disappear completely, but the entanglement still exists, which is the consequence of the stricter quantum correlation of steering than of entanglement. The bipartite steering S_{rp}, S_{pr} versus $\varepsilon_1/\varepsilon_2$ with $\gamma_{pq} = 0.35\kappa_{pq}$ is depicted in Fig. 5(e). When the driving satisfies $\varepsilon_1 < 0.46\varepsilon_2$,

asymmetric steering can be obtained (yellow region), in which the steerable ability of the skyrmion to control the p-mode magnon is stronger than that of the p-mode magnon to the skyrmion ($S_{rp} > S_{pr}$). As ε_1 continues to increase, only the skyrmion can control the state of p-mode magnon, but the latter will not affect the skyrmion. From Fig. 5(f), it can be seen that the asymmetric steering is generated for the temperature below 0.1 K, the one-way steering S_{rp} still survives when $T = 0.29$ K, and the entanglement shows strong robustness against the temperature ($T < 0.76$ K).

Figure 6(a) shows the quantum correlation E_{rq}, S_{rq}, S_{qr} as functions of $\varepsilon_1/\varepsilon_2$ with $\varepsilon_2 = 0.01 \times 10^8$ Hz. In Fig. 6(a), the entanglement is generated in the range of $\varepsilon_1/\varepsilon_2 < 93$ and the one-way steering from the difference-frequency magnon to the skyrmion can stably exist for $\varepsilon_1/\varepsilon_2 < 76$ ($S_{qr} > 0, S_{rq} = 0$, blue region). From Fig. 6(b), it can be found that E_{rq} can be strengthened by increasing the driving ε_1 with large sum (difference)-frequency magnon dissipation. Notably, steering from the skyrmion to the q-mode magnon is generated for high damping when $\gamma_{pq} > 2.3\kappa_{pq}$ ($S_{rq} > 0$), and similarly it can be enhanced by changing the dissipation γ_{pq} and the driving amplitude ε_1, which is shown in Fig. 6(c). Different from that, S_{qr} will decrease with the addition of γ_{pq}, which means the magnon dissipation plays a destructive role in the steering S_{qr} in Fig. 6(d). Moreover, steering direction can be flexibly manipulated by the driving amplitude ε_1, which is shown in Fig. 6(e). When $0 < \varepsilon_1/\varepsilon_2 < 51$, there is the one-way steering S_{rq} (red region), in which the state of the q-mode magnon can be unidirectionally controlled by applying measurements on the skyrmion. As the driving ε_1 increases, two-way steering can be obtained with $51 < \varepsilon_1/\varepsilon_2 < 61$ (yellow region). Although two magnons can affect the state of the other side, S_{rq} is larger than S_{qr}, which indicates a stronger steerable ability from the skyrmion to the q-mode magnon with the parameter regime $51 < \varepsilon_1/\varepsilon_2 < 58.7$, but when the driving satisfies the condition $58.7 < \varepsilon_1/\varepsilon_2 < 61$, the steering direction is reversed and the steering from the q-mode magnon to the skyrmion is dominant ($S_{qr} > S_{rq}$). When ε_1 continues to increase and is less than $106\varepsilon_2$, the system only has one-way steering from the q-mode magnon to the skyrmion (blue region). In Fig. 6(f), the survival temperatures of the steering S_{rq}, S_{qr} are 0.15 K and 0.13 K, respectively. The ability of the skyrmion to steer the q-mode magnon is more robust against thermal noise. The entanglement does not disappear until the temperature is greater than 0.78 K.

Furthermore, the genuine tripartite entanglement among the skyrmion, the sum- and difference-magnons can be achieved at the steady state, which is numerically demonstrated in Fig. 7(a) ($R_\tau^{\min} > 0$). It can be seen that the tripartite entanglement appears when the driving $\varepsilon_2 > 0.24 \times 10^8$ Hz and the entanglement can be significantly enhanced by increasing the driving amplitude ε_2. In the case of the low driving amplitude ε_2 ($(0.05\text{–}0.15) \times 10^8$ Hz), a genuine tripartite entangled state also can be generated in the system by controlling the driving ε_1 where the three magnons are entangled with each other [E_{rp}, E_{rq}, $E_{pq} > 0$, see Figs. 2(b)–2(d)]. Moreover, as shown in Fig. 3, the mWGM, the skyrmion, the sum-frequency and the difference-frequency magnons can be simultaneously entangled with each other in some parameter intervals, which indicates the potential existence of quadripartite entanglement in the system. Figure 7(b) depicts the influence of the magnon dissipation and environment temperature on the tripartite entanglement for $\varepsilon_{1(2)} = 0.3(0.5) \times 10^8$ Hz. It is clear that the magnon damping and the thermal noise are destructive to the tripartite entanglement, yet it can exist when the temperature is less than 0.42 K and $\gamma_{p(q)} < 2\kappa_{p(q)}$. Since quantum effects such as entanglement and steering in the system need to be prepared under the condition of small enough thermomagnon numbers, the survival temperature of entanglement is dependent on the magnon working frequency, as indicated by the formula of the equilibrium average thermal magnon number in Section 2. Theoretically, the tripartite entanglement could be prepared in the temperature of several tens of Kelvin for THz MFC in antiferromagnets.[26,27]

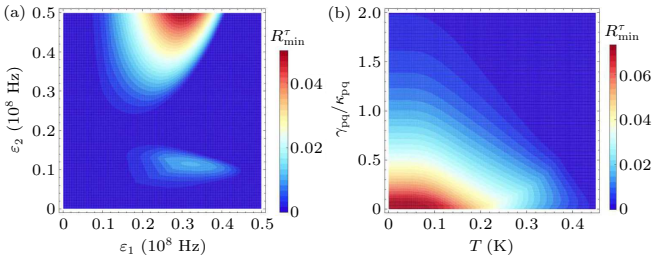


Fig. 7. Density plot of genuine tripartite entanglement $R_{\min}^{\tau}$ among the skyrmion, sum- and the difference-frequency magnon modes versus (a) two drivings ε_1 and ε_2, (b) the temperature T and the magnon dissipation γ_{pq} with $\varepsilon_1 = 0.13 \times 10^8$ Hz and $\varepsilon_2 = 0.5 \times 10^8$ Hz.

4. Conclusion

In conclusion, we have investigated how to create and control the multipartite entanglement and one-way steering in an MFC based on nonlinear magnon–skyrmion scattering. When the mWGM and the skyrmion are driven by two microwave fields, respectively, the skyrmion can be entangled with three magnon teeth of the MFC and the entanglement between the sum- and difference-frequency magnons exists simultaneously. It is found that the entanglements of different subsystems are strongly dependent on the amplitudes of two driving fields, which is triggered by the fact that the amplitudes will affect the effective coupling strength among different magnon modes. The perfect one-way steering from the skyrmion to the mWGM and the sum-frequency magnon and

from the difference-frequency magnon to the skyrmion can be obtained in the system. Intriguingly, the asymmetric steering of the three bipartitions occurs with appropriate magnon dissipations, in which the steerable direction of the skyrmion and the first-order two magnons could be performed in a controllable manner by changing two driving amplitudes not requiring added noise. Additionally, genuine tripartite entanglement among the skyrmion and the first-order magnon pair in the MFC can be realized and it could be significantly strengthened by enhancing the driving on the skyrmion. The steady-state bipartite and tripartite entanglements are robust against external thermal fluctuations.

Considering more higher-order magnons in the MFC, multi-mode entanglement among different magnon combs could be anticipated. Our work enriches the research of multipartite quantum correlations in MFCs, which may be significant for the application in quantum communication and computation networks. On the other hand, because the working frequencies of magnons and microwave photons are both in the microwave frequency band, they can couple with each other when they satisfy the matching conditions of momentum and energy. This coupling can be further extended to cavity magnonics systems. By utilizing the virtual photon excitation in the microwave field, the coupling with superconducting qubits could be realized. In addition, optical photons can couple with the mWGM via Brillouin scattering. This opens up exciting prospects for the development of hybrid magnon-based systems, potentially creating new platforms for exploring novel magnon phenomena.

Acknowledgments

Project supported by the National Key R&D Program of China (Grant No. 2022YFA1402802) and the National Natural Science Foundation of China (Grant Nos. 12374103, 12434003, and 12074057).

References

[1] Horodecki R, Horodecki P, Horodecki M and Horodecki K 2009 *Rev. Mod. Phys.* **81** 865
[2] Caleffi M, Amoretti M, Ferrari D, Illiano J, Manzalini A and Cacciapuoti A S 2024 *Computer Networks* **254** 110672
[3] Ren J G, Xu P, Yong H L, Zhang L, Liao S K, Yin J, Liu W Y, Cai, W Q, Yang M, Li L, *et al.* 2017 *Nature* **549** 70
[4] Yin J, Li Y H, Liao S K, Yang M, Cao Y, Zhang L, Ren J G, *et al.* 2020 *Nature* **582** 501
[5] Cavalcanti D and Skrzypczyk P 2017 *Rep. Prog. Phys.* **80** 024001
[6] Uola R, Costa A C, Nguyen H C and Gühne O 2020 *Rev. Mod. Phys.* **92** 015001
[7] Branciard C, Cavalcanti E G, Walborn S P, Scarani V and Wiseman H M 2012 *Phys. Rev. A* **85** 010301
[8] Kocsis S, Hall J M, Bennet A J, Saunders J D and Pryde J G 2014 *Nat. Commun.* **6** 5886
[9] Walk N, Hosseini S, Geng, J, Thearle O, Haw J Y, Armstrong S, Assad S M, Janousek J, Ralph T C, Symul T, Wiseman H M and Lam P K 2016 *Optica* **3** 634
[10] Wang M H, Xiang Y, Kang H J, Han DM, Liu Y, He Q Y, Gong Q H, Su X L and Peng K C 2020 *Phys. Rev. Lett.* **125** 260506
[11] Jones B D, Šupić I, Roope U, Nicolas B and Paul S 2021 *Phys. Rev. Lett.* **127** 170405
[12] Barreiro J T, Bancal J D, Schindler P, Nigg D, Hennrich M, Monz T, Gisin N and Blatt R 2013 *Nat. Phys.* **9** 559
[13] Armstrong S, Wang M, Teh R Y, Gong Q H, He Q Y, Janousek J, Bachor H A, Reid M D and Lam P K 2015 *Nat. Phys.* **11** 167
[14] Kunkel P, Prüfer M, Strobel H, Linnemann D, Frölian A, Gasenzer T, Gärttner M and Oberthaler M K 2018 *Science* **360** 413
[15] Hao Z Y, Sun K, Wang Y, Liu Z H, Yang M, Xu J S, Li C F and Guo G C 2022 *Phys. Rev. Lett.* **128** 120402
[16] Teh R Y, Gessner M, Reid M D and Fadel M 2022 *Phys. Rev. A* **105** 012202
[17] Kues M, Reimer C, Lukens M J, Munro J W, Weiner M A, Moss J D and Morandotti R 2019 *Nat. Photon.* **13** 170
[18] Pysher M, Miwa Y, Shahrokhshahi R, Bloomer R and Pfister O 2011 *Phys. Rev. Lett.* **107** 030505
[19] Chen M, Menicucci N C and Pfister O 2014 *Phys. Rev. Lett.* **112** 120505
[20] Reimer C, Kues M, Roztocki P, Wetzel B, Grazioso F, Little E B, Chu T S, Johnston T, Bromberg Y, Caspani L, Moss J D and Morandotti R 2016 *Science* **351** 1176
[21] Wang Z Y, Yuan H Y, Cao Y S, Li Z X, Duine R A and Yan P 2021 *Phys. Rev. Lett.* **127** 037202
[22] Hula T, Schultheiss K, Gonçalves F J T, Körber L, Bejarano M, Copus M, Flacke L, Liensberger L, Buzdakov A, Kákay A, Weiler M, Camley R, Fassbender J and Schultheiss H 2022 *Appl. Phys. Lett.* **121** 112404
[23] Xu G T, Zhang M, Wang Y, Shen Z, Guo G C and Dong C H 2023 *Phys. Rev. Lett.* **131** 243601
[24] Wang C Y, Rao J W, Chen Z J, Zhao K X, Sun L X, Yao B M, Yu T, Wang Y P and Lu W 2024 *Nat. Phys.* **20** 1139
[25] Zhang Y L, Sheng L T, Chen J L, Wang J, Zhu Z T, Yuan R D, Lu J D, Wang H C, Hao, S J, Chen P, Yu G Q, Han X F and Yu H M 2023 *Chin. Phys. B* **32** 107505
[26] Yao X L, Jin Z J Y, Wang Z Y, Zeng Z Z and Yan P 2023 *Phys. Rev. B* **108** 134427
[27] Zhang C X, Jin Z J Y, Liu X J and Yan P 2024 *Appl. Phys. Lett.* **125** 052401
[28] Liu Y, Liu T T, Yang Q Q, Tian G, Hou Z P, Chen D Y, Fan Z, Zeng M, Lu X B, Gao X S, Qin M H and Liu J M 2024 *Phys. Rev. B* **109** 174412
[29] Abdulrazak T, Liu X J, Jin, Z J Y, Cao Y S and Yan P 2024 *Chin. Phys. B* **33** 087503
[30] Liu Z X 2024 *Appl. Phys. Lett.* **124** 032403
[31] Verba R, Körber L, Schultheiss K, Schultheiss H, Tiberkevich V and Slavin A 2021 *Phys. Rev. B* **103** 014413
[32] Qu T, Hamill A, Victora R H and Crowell P A 2023 *Phys. Rev. B* **107** L060401
[33] Schultheiss H, Vogt K and Hillebrands B 2012 *Phys. Rev. B* **86** 054414
[34] Wang Y P, Zhang G Q, Zhang D K, Luo X Q, Xiong W, Wang S P, Li T F, Hu C M and You J Q 2016 *Phys. Rev. B* **94** 224410
[35] Wang Y P, Zhang G Q, Zhang D K, Li T F, Hu C M and You J Q 2018 *Phys. Rev. Lett.* **120** 057202
[36] Zhang G Q, Wang Y P and You J Q 2019 *China Phys. Mech. Astron.* **62** 987511
[37] Wu W J, Xu D, Qian J, Li Jie, Wang, Wang Y P and You J Q 2022 *Chin. Phys. B* **31** 127503
[38] Wang X, Huang K W, Qiu Q Y and Xiong H 2023 *Chaos, Solitons & Fractals* **176** 114137
[39] Jolin S W, Andersson G, Rivera Hernández J C, Strandberg I, Quijandría F, Aumentado J, Borgani R, Tholén M O and Haviland D B 2023 *Phys. Rev. Lett.* **130** 120601
[40] Zheng Q J, Yuan H Y, Cao Y S and Yan P 2025 *Phys. Rev. B* **111** 214433
[41] DeJesus E X and Kaufman C 1987 *Phys. Rev. A* **35** 5288
[42] Vitali D, Gigan S, Ferreira A, Böhm H R, Tombesi P, Guerreiro A, Vedral V, Zeilinger A and Aspelmeyer M 2007 *Phys. Rev. Lett.* **98** 030405
[43] Adesso G, Serafini A and Illuminati F 2004 *Phys. Rev. A* **70** 022318
[44] Kogias I, Lee A R, Ragy S and Adesso G 2015 *Phys. Rev. Lett.* **114** 060403
[45] Adesso G and Illuminati F 2006 *New J. Phys.* **8** 15